Lazarus Godson Asirvatham[1]
Department of Mechanical Engineering,
Karunya University,
Coimbatore 641 114, India
e-mails: godson@karunya.edu;
godasir@yahoo.co.in

Somchai Wongwises
Fluid Mechanics,
Thermal Engineering and Multiphase Flow
Research Laboratory (FUTURE),
Department of Mechanical Engineering,
Faculty of Engineering,
King Mongkut's University
of Technology Thonburi,
Bangmod, Bangkok 10140, Thailand
e-mail: somchai.won@kmutt.ac.th

Jithu Babu
Department of Mechanical Engineering,
Karunya University,
Coimbatore 641 114, India
e-mail: Jithubabu90@gmail.com

Heat Transfer Performance of a Glass Thermosyphon Using Graphene–Acetone Nanofluid

This study presents an enhancement in the heat transfer performance of a glass thermosyphon using graphene–acetone nanofluid with 0.05%, 0.07%, and 0.09% volume concentrations. The heat load is varied between 10 and 50 W in five steps. The effect of heat load, volume concentration, and vapor temperature on thermal resistance, evaporator and condenser heat transfer coefficients, are experimentally investigated. A substantial reduction in thermal resistance of 70.3% is observed for the maximum concentration of 0.09% by volume of graphene–acetone nanofluid. Further, an enhancement in the evaporator heat transfer coefficient of 61.25% is observed for the same concentration. Also from the visualization study the different flow patterns in the evaporator, adiabatic, and condenser regions are obtained for acetone at different heat inputs.
[DOI: 10.1115/1.4030479]

Keywords: acetone, graphene, nanoparticles, thermosyphon, convection, heat transfer

1 Introduction

Thermosyphons are two-phase heat transfer devices, suitable to transfer heat from the source to the sink, due to the phase change of the working fluid assisted by gravity effect. The evaporator section is filled with certain amount of working fluid which vaporizes, when the heat input is supplied and the vapor passes through the adiabatic section and gets condensed in the condenser section. The condensed liquid falls back to the evaporator through the walls of the thermosyphon due the action of gravity. Thermosyphons are used in many applications [1,2] for dissipating heat from various engineering systems including electronic cooling like computers, laptops, notepads and also in solar energy systems, air cooling, waste heat recovery, and in air preheating systems. For decades the application of thermosyphon in thermal management have been studied and they are proven to be an effective, reliable, light-weight, low-cost heat transfer device. However, the use of convectional heat transfer fluids such as deionized (DI) water, methanol, ethanol, etc., in thermosyphon possess limited heat transfer capabilities [3], since the thermal conductivity of these conventional fluids is very low when compared with that of the solids. The use of these low thermal conductive fluids in thermosyphons is a limitation to meet the present day heat removal requirement of modern electronic devices. The idea is to disperse solid nanoparticles in the working fluid to overcome this limitation and to improve the thermal conductivity. Thus, the nanofluids emerged as an alternative for convectional heat transfer fluids. Studies [4,5] proved that the use of nanofluid reduces the thermal resistance and there by increases the thermal conductivity. Longo and Zilio [6] measured thermal conductivity of Al_2O_3–water (1–4% particle volume concentration) and TiO_2–water (1–6% particle volume concentration) nanofluid at temperature ranging from 1 to 40 °C, using transient hot disk TPS 2500 S apparatus having a maximum uncertainty of k is equal to 2 W/mK, lower than ±5.0% of the reading. The result showed that the thermal conductivity enhanced from −2 to 16% and from −2 to 23% with reference to pure water. Baby and Ramaprabhu [7] measured the thermal conductivity of graphene/DI water nanofluid for temperature ranging from 25 °C to 50 °C using the Decagon KD2 Pro thermometer. The probe sensor used for these measurements is of length 6 cm and of diameter 1.3 mm. The overall uncertainty in thermal conductivity was less than 4% including temperature variation. The result showed an enhancement in thermal conductivity by about 14% at 25 °C with DI water as the base fluid at a very low volume fraction of 0.056% and increases about 64% at 50 °C. The factors affecting the thermal conductivity of nanofluid include the particle size, temperature, volume fraction, and interfacial layer [8]. To ensure optimal and stable steady-state operation, the thermosyphon should be optimally filled. An optimally filled thermosyphon has shorter response time and lowest thermal resistance and it also prevents breakdown of the liquid film [9].

Noie et al. [10] investigated the heat transfer enhancement of two-phase closed thermosyphon (TPCT) using pure water and nanofluids of aqueous Al_2O_3 nanoparticles suspensions with various volume concentrations varying from 1–3%. The TPCT made of copper tube with internal diameter of 20 mm, 1 mm thickness, and 1000 mm in length of which evaporator and condenser sections had 350 and 400 mm length were used. The electric heaters around the evaporator section were made of a nickel-chrome wire having nominal power of 1000 W. Experimental results showed that for different heat input powers, the efficiency of the TPCT increases up to 14.7% when Al_2O_3/water nanofluid was used instead of pure water. It was reported that the thermal resistance of the TPCT when charged with nanofluids was found to be less. It was suggested that the heat transfer enhancement in TPCT by nanofluid greatly depends on particle type, particle size, base fluid, and bubble nucleation size.

Huminic et al. [11] investigated the thermal performance by the use of solid nanoparticles added to water as the working fluid in a thermosyphon. The thermosyphon made of copper tube of 15 mm outer diameter and 2000 mm in length was used. The temperature of heating water from the evaporator section was kept constant by a thermostatic bath (GD 120-S26) and the operating temperature varied between 50 and 90 °C. However, the cooling water from the condenser was kept constant at 20 °C by a thermostatic bath (Haake C10-P5/U) with an uncertainty of ±0.04 °C. The tested concentration levels of nanoparticles were 2% and 5.3%, and the

[1]Corresponding author.

Contributed by the Heat Transfer Division of ASME for publication in the Journal of Heat Transfer. Manuscript received May 3, 2014; final manuscript received March 3, 2015; published online July 14, 2015. Assoc. Editor: Bruce L. Drolen.

results showed that the addition of 5.3% (by volume) of iron oxide nanoparticles in water showed improvement in thermal performance compared with the operation with DI-water. Kang et al. [12] investigated the thermal performance of a conventional 211 μm wide $\times$ 217 μm deep grooved circular heat pipe with 35 nm diameter silver nanoparticles dispersed in water as a working fluid. The tested silver nanoparticles concentrations ranged from 1 mg/l to 100 mg/l. The results showed that the thermal resistance decreased 10–80% compared to DI-water for an input power of 30–60 W. The study also reported that the thermal resistances of the heat pipe decreased as the silver nanoparticles size and concentration increased. Asirvatham et al. [13] investigated heat transfer performance of silver nanoparticles with very low volume concentration ranged from 0.003% to 0.009% with an average nanoparticles diameter of 58.35 nm in heat pipe. The reported results showed a reduction in thermal resistance of 76.2% for 0.009 vol. % concentration of silver nanoparticles. Further, an enhancement in the evaporation heat transfer coefficient of 52.7% was observed for the same concentration. The use of nanoparticles enhanced the operating range of heat pipe by 21% compared with that of DI water.

Karthikeyan et al. [14] experimentally investigated the thermal performance of TPCT using distilled water and aqueous solution at different inclinations. The thermosyphon was tested for the inclinations of 45 deg, 60 deg, and 90 deg to the horizontal. A copper thermosyphon having a length of 1000 mm, with an inner and outer diameter of 17 mm and 19 mm with evaporator and condenser lengths of 400 mm and 450 mm were used. The thermosyphon was tested for different heat inputs ranged between 40 W, 60 W, and 80 W with an evaporator charge ratio of 60%. Results showed that the efficiency of thermosyphon is better for aqueous solution than that of the distilled water for all inclinations, heat input and flow rates. The efficiency was higher in vertical position than in the inclined position. The lower inclination reduced the efficiency due to the obstruction of vapor with condensate return from the condenser. The efficiency was higher for 40 W heat input than at 60 W and 80 W heat inputs. Mozumder et al. [15] tested the thermal resistance and overall heat transfer coefficient of a miniaturized heat pipe with 5 mm diameter and 150 mm length heat pipe with water, methanol, and acetone as the working fluid with 35%, 55%, and 100% filling ratios. The heat pipe was tested at different heat load raging from 2 W to 10 W with an increment of 2 W. The result showed that the overall heat transfer was higher for acetone and the thermal resistance was lower. It was reported that 100% fill ratio of evaporator volume showed a best result with minimum temperature difference across the evaporator and condenser for acetone. It was suggested that, generally the fill ratios of working fluid greater than 85% of volume of evaporator show better results in terms of increased heat transfer coefficient, decreased thermal resistance, and reduced temperature difference across the evaporator and condenser. Naphon and Assadamongkol [16] experimentally investigated the performance of heat pipe by the use of nanoparticles suspended in refrigerant and found that the heat pipe with 0.1% concentration of nanoparticles operated with efficiency 1.40 times higher than that with pure refrigerant.

It has been clearly observed from the above mentioned literature that the studies on heat transfer performance of thermosyphons using nanofluids are relatively small. It was also observed that most of the previous works that have been performed to find the heat transfer performance of thermosyphon made of copper or aluminum material. Since the copper and aluminum are not transparent, it is not possible to visualize the two-phase moment of the heat transfer fluid from the evaporator to the condenser inside the thermosyphon. Moreover, all the previous experiments have been conducted by measuring only the wall temperature to evaluate the heat transfer performance of thermosyphon and, so far no work has been reported till date to measure the vapor temperature inside a thermosyphon in the evaporator and in the condenser regions to predict the difference between the wall and vapor temperature and to find out the convective heat transfer coefficient in evaporator and condenser sections. Also, no visualization study has been reported to realistically visualize two-phase flow pattern inside a thermosyphon. For this purpose, a low boiling working fluid (acetone) is chosen as the heat transfer fluid. The boiling point of acetone at standard atmospheric pressure is 56 °C. Since the pressure maintained inside the thermosyphon is below 0.5 bar, so the acetone boils even at a temperature below 40 °C. Hence the present study aims at manufacturing a thermosyphon made of borosilicate glass to know what is happening inside a thermosyphon, and to visualize the two-phase flow pattern in the evaporator, adiabatic, and condenser sections at different heat loads. Some visualization study [17] was performed in closed loop pulsating heat pipe with R-123 as working fluid. The knowledge of flow pattern in a thermosyphon is essential to understand the heat transfer characteristics when designing the thermosyphon according to the specific application. Hence a dedicated visualization study of the flow pattern in a two-phase thermosyphon is conducted with acetone as the working fluid. Also the thermal performance of glass thermosyphon with acetone and graphene–acetone nanofluids with 0.05%, 0.07%, and 0.09% volumetric concentrations with heat load varying from 10 W to 50 W are studied. The effect of heat load on the quantities such as thermal resistance, axial temperature distribution, evaporation, condensation heat transfer coefficients, effective thermal conductivity, etc., are experimentally analyzed on the basis of vapor core and wall temperatures and presented.

2 Experimentation

2.1 Experimental Setup. The study of heat transfer performance and visualization of flow patterns at different heat inputs are performed using the experimental setup shown in Fig. 1. The experimental setup consists of glass thermosyphon filled with working fluid, water-cooled condenser section, thermocouples, heater connected to a variac, glass wool insulation, and data logger connected to a computer. The thermosyphon is made of borosilicate glass that has an outside diameter of 12 mm and a wall thickness of 2 mm. The total length of heat pipe (310 mm) is divided into an evaporator section of 90 mm, adiabatic section of 100 mm, and condenser section of 120 mm. The length of condenser section is selected in such a way that its length is sufficient enough to

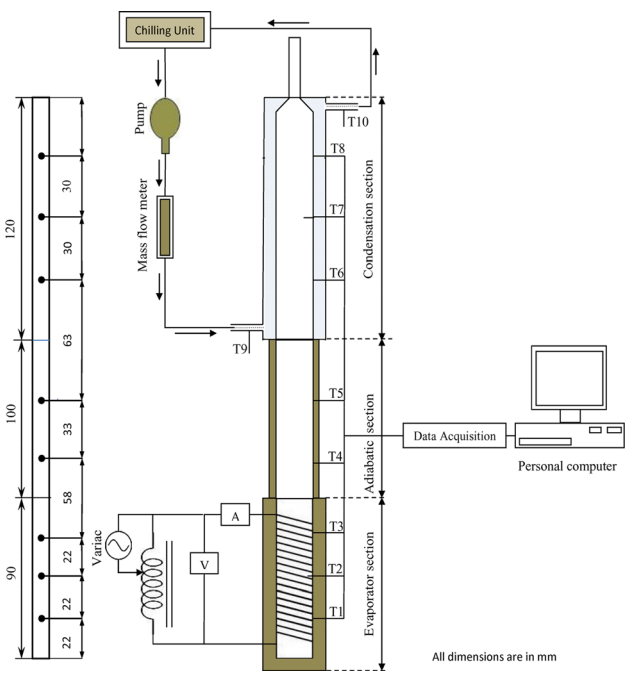

Fig. 1 Schematic diagram of experimental setup

condense all the vapors coming to it. A charging ratio equal to 80% of the evaporator volume is used for both working fluids. The condenser is also made of borosilicate glass, and it enclosed the condenser section of the heat pipe. Cooling water kept a constant temperature of 25°C with the help of a chilling unit and is used as the coolant. The constant flow of coolant (205 ml per minute) is maintained using a pump, and the flow rate is measured with a flow meter having an uncertainty of ±10 ml. To measure the temperatures at different regions of the heat pipe, cooling water inlet, and cooling water outlet, eight T-type thermocouples are used. The positions of the thermocouples have been clearly indicated in Fig. 1. These thermocouples have an uncertainty of ±0.5°C. The thermocouples on the heat pipe are fixed so that they will give the outer wall temperature of the heat pipe. The vapor temperatures at the evaporator and condenser are also measured by inserting thermocouples into the heat pipe, and the places where thermocouples are inserted were properly sealed to maintain the vacuum inside the heat pipe. Two thermocouples were used at each section of the heat pipe to measure the wall temperatures. Cooling water inlet and outlet temperatures are measured using T_9 and T_{10} thermocouples. To give the heat input to the evaporator, a heater coil is wound around the evaporator which, in turn, is connected to a variac with wattmeter having an uncertainty of ±0.5 W. An AC supply of 220 V is used as the power source. The thick layer of glass wool insulation is used to prevent any heat losses from the heat pipe to the ambient. All temperatures measured at different heat loads are recorded in a computer by connecting a data logger in between the thermocouples and computer. A data logger of Model-(DA100-13-1F), Yokogawa-N 200 is used for this purpose. For visualization of the flow patterns in the heat pipe at different heat loads, a Canon 60D DSLR camera is used.

2.2 Experimental Procedure

2.2.1 Nanofluid Preparation. The graphene–acetone nanofluid is prepared by a two-step method that involves adding graphene nanoparticles into acetone and mixing it with a sonicator. The graphene nanoparticles used in this study were purchased from Skyspring Nanomaterials (Houston, TX), with the product number 0541DX. The size of nanoparticles is in the range of set 6–8 nm. The volume fractions used in this study are 0.05, 0.07, and 0.09%. The mass of nanoparticles corresponding to the volume concentration is measured using a weight balance that can measure weight as low as 0.001 g. No surfactant is used in the preparation of the nanofluid. The sonicator used in this study has a sound frequency of 85–95 kHz. The graphene–acetone mixture sonicated for 25 minutes gives the nanofluid. The nanofluid prepared for a volume fraction of 0.009% is used for the stability test. Photos taken for seven hours on seven days are shown in Fig. 2. From the visual observation, it can be seen that the graphene–acetone nanofluid is very stable for seven days. So it is assumed that the nanofluid is stable throughout the experiments. The nanofluid is prepared just before the filling process, and the heat pipe is immediately tested after filling. Characterization of nanoparticles is done using scanning electron microscope (SEM) images. One image taken at a magnification of 1500X for 0.09% volume concentration is shown in Fig. 3. The image clearly indicates some amount of agglomeration in the nanofluid even though nanoparticles are well distributed in acetone. The spread-out sheet-like structure of graphene is also clearly visible in the SEM image.

2.2.2 Performance Test. The experiments are conducted using four identical thermosyphons in vertical position, which are fabricated as per the mentioned dimensions in Fig. 1. One of the thermosyphons is filled with acetone, and the remaining three thermosyphons are filled with three different volume concentrations of graphene–acetone nanofluid. All four thermosyphons are tested under identical operating conditions, such as inlet temperature, mass flow rate of the cooling water circulating through the condenser section, and the power input to the evaporator. The steady-state vapor and wall temperature readings are recorded using a data acquisition system. The input heat load is incremented gradually in equal steps from 10 to 50 W.

2.2.3 Visualization Study. Visualization of the flow pattern is carried out by using the glass thermosyphon with acetone as the working fluid. The thermosyphon is placed vertically, and the cooling water is circulated at a constant flow rate of 205 ml per minute through the condenser section and a constant temperature chilled water bath is used to maintain the inlet temperature of the circulating cooling water in the condenser at 25°C for various heat loads. The heat input is supplied to the thermosyphon using a digital wattmeter connected to an electric heater wound on the evaporator section. A high-resolution Canon 60D DSLR camera is used to record the flow pattern inside the evaporator, adiabatic, and condenser section of the thermosyphon for a heat load from 10 to 50 W.

2.3 Data Reduction. The performance of a heat pipe can be determined by calculating its thermal resistance. Thermal resistance is the ratio of temperature difference between the evaporator and condenser to the applied heat load as given in Eq. (1). In the case of a thermosyphon heat pipe, the temperatures are wall temperatures of the evaporator and condenser and the heat transferred is the applied heat load. Thermal resistance of thermosyphon (R_T) is given by

$$R_T = \frac{T_{e,w} - T_{c,w}}{Q} \tag{1}$$

The heat transfer coefficient at the evaporator is another term used to compare the heat transfer at the evaporator section of the thermosyphon. The equation of the heat transfer coefficient comes from the equation of convective heat transfer. In the evaporator, heat is transferred from the evaporator wall to the working fluid. The temperatures of the surface ($T_{e,s}$) and vapor ($T_{e,v}$) at the evaporator are used to calculate the heat transfer coefficient using Eq. (2). The evaporator heat transfer coefficient (h_e) is given by

$$h_e = \frac{Q}{A_e \Delta T_e} \tag{2}$$

where

$$A_e = \pi d_e l_e \quad \Delta T_e = T_{e,s} - T_{e,v}.$$

The heat transfer coefficient at the condenser is calculated using the temperatures of vapor and surface at the condenser section of the thermosyphon using Eq. (3). Here, the vapor temperature will be higher than that of the condenser surface temperature. So the heat transfer coefficient at condenser (h_c) is calculated as

$$h_c = \frac{Q}{A_c \Delta T_c} \tag{3}$$

where

$$A_c = \pi d_c l_c \quad \Delta T_c = T_{c,v} - T_{c,s}$$

where ($T_{c,v}$) is the vapor temperature and ($T_{c,s}$) is the surface temperature at the condenser.

The thermal conductivity of the heat pipe corresponding to the thermal resistance, area of cross section, and length is called the effective thermal conductivity of the heat pipe, as given in Eq. (4). The effective thermal conductivity K_{eff} of the heat pipe is calculated as

$$K_{eff} = \frac{1}{A_{c/s,T} R_T} \tag{4}$$

where ($A_{c/s,T}$) is the cross-sectional area of the thermosyphon.

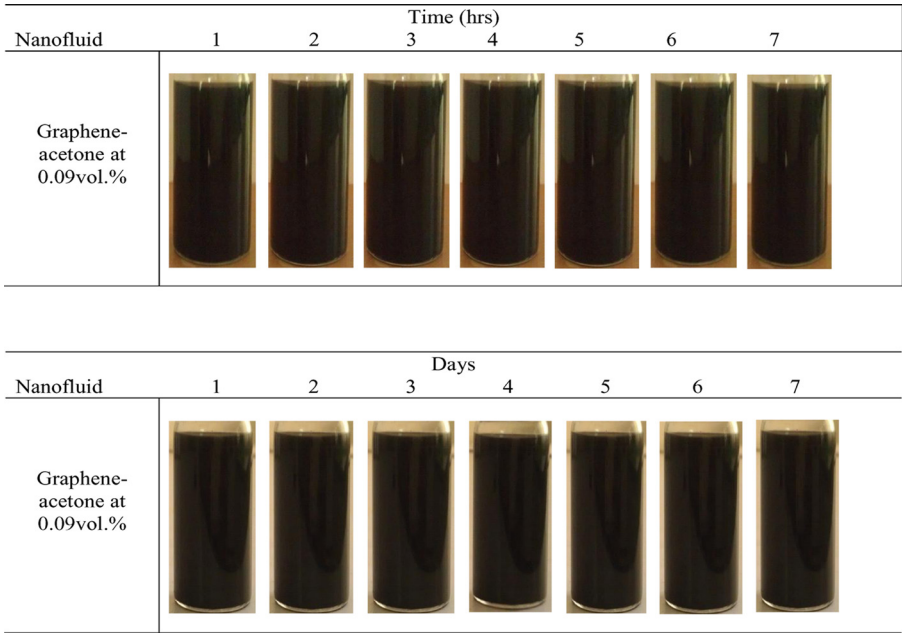

Fig. 2 Photos of visualization for acetone–graphene nanofluid at 0.09 vol. %

2.3.1 Uncertainty Analysis of Measured Parameters. The uncertainty in heat flux given in Eq. (5) is calculated based on the uncertainties in the applied voltage (ΔV), applied current (ΔI) to the heater coil, uncertainties in the diameter (Δd_e), and measured length (Δl_e) of the evaporator section. The vernier caliper is used to measure the length and diameter of the thermosyphon and the least count of the vernier calipers is taken as the uncertainty value

$$\frac{\Delta q}{q} = \sqrt{\left(\frac{\Delta V}{V}\right)^2 + \left(\frac{\Delta I}{I}\right)^2 + \left(\frac{\Delta I_e}{I_e}\right)^2 + \left(\frac{\Delta d_e}{d_e}\right)^2} \tag{5}$$

Similarly, the uncertainty in the thermal resistance given in Eq. (6) depends on the uncertainty in the applied heat (ΔQ) and uncertainty in the measured temperature difference between evaporator and condenser ($U(\Delta T)$). The actual measured temperature difference is denoted as (ΔT_{ec})

$$\frac{\Delta R}{R} = \sqrt{\left(\frac{\Delta Q}{Q}\right)^2 + \left(\frac{\Delta(\Delta T)}{\Delta T_{ec}}\right)^2} \tag{6}$$

$$\frac{\Delta h}{h} = \sqrt{\left(\frac{UQ}{Q}\right)^2 + \left(\frac{U\Delta T}{\Delta T_{vs}}\right)^2} \tag{7}$$

Finally, the uncertainty in the heat transfer coefficient given in Eq. (7) is calculated by taking into account the uncertainty in the applied heat load (UQ) and uncertainty in the measured temperature difference between surface and vapor ($U\Delta T$). All these calculations are done to eliminate the experimental errors and the obtained results are taken from a standardized experimental test facility. The maximum uncertainties in thermal resistance and heat transfer coefficient are found to be 5.98% and 6.82%.

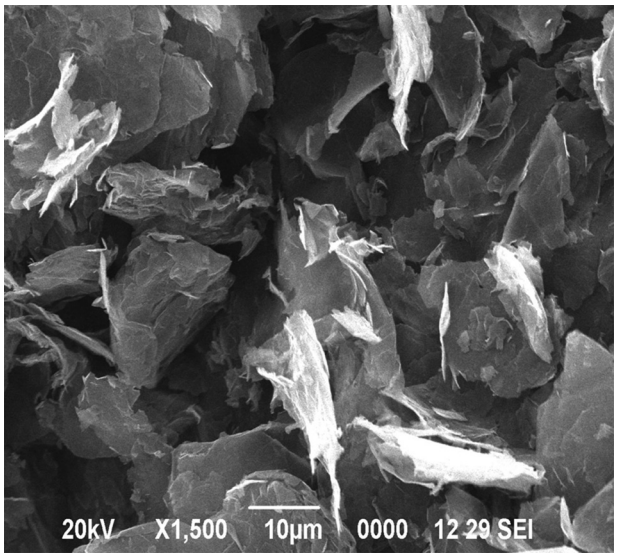

Fig. 3 SEM image of 0.09 vol. % of acetone–graphene nanofluid

2.4 Thermophysical Properties of Nanofluid. The density of the graphene–acetone nanofluid is calculated using Pak and Cho [18] equation

$$\rho_{nf} = \varphi\rho_p + (1-\varphi)\rho_A \tag{8}$$

Similarly, the thermal conductivity of graphene–acetone nanofluid is calculated using the following Eq. (9) proposed by the present authors [19]:

Table 1 Experimental conditions

Working fluid charge (ml)	Q (W)	m_w (kg/s)	$T_{w\ inlet}$ (°C)
5.6	10	0.00341	25
	20	0.00341	25
	30	0.00341	25
	40	0.00341	25
	50	0.00341	25

Table 2 Evaporator wall and vapor temperatures (°C)

	Acetone		0.05 vol. %		0.07 vol. %		0.09 vol. %	
Q(W)	TE, wall	TE, vap	TE, wall	TE, vap	TE, wall	TE, vap	TE, wall	TE, vap
10	43.1	40.0	42.1	40.8	41.7	40.6	40.0	39.0
20	51.5	46.3	47.8	45.4	44.9	42.8	42.3	40.5
30	55.9	51.6	51.3	47.9	51.3	48.8	49.3	47.3
40	66.1	61.1	56.4	52.1	54.0	51.1	52.1	49.9
50	72.1	66.6	60.0	55.0	58.6	55.7	54.7	52.7

Table 3 Condenser vapor and wall temperatures (°C)

	Acetone		0.05 vol. %		0.07 vol. %		0.09 vol. %	
Q (W)	TC, vap	TC, wall	TC, vap	TC, wall	TC, vap	TC, wall	TC, vap	TC, wall
10	32.4	28.1	33.3	29.1	33.0	28.9	34.5	30.8
20	41.0	31.9	39.8	30.9	38.4	29.8	40.0	31.8
30	48.2	33.7	46.5	32.4	47.1	33.5	46.3	33.7
40	59.0	38.0	53.9	33.8	52.7	33.5	51.9	34.7
50	66.2	39.1	60.2	34.7	58.9	34.8	57.7	35.1

$$\frac{k_{nf}}{k_A} = 0.877\left(\frac{T_F}{T_\alpha}\right)^{0.837} + \varphi^{0.34} \tag{9}$$

3 Results and Discussion

3.1 Performance Test. The experiments are conducted for various heat inputs (10 W, 20 W, 30 W, 40 W, and 50 W) with thermosyphon kept in vertical position. The vapor and the surface temperature readings are obtained using the thermocouple connected to the data acquisition system. The experimental results are compared between acetone and the graphene–acetone nanofluids for the tested concentrations. The observed enhancement is the heat transfer performance due to the increase in the volume concentration of graphene nanofluid, heat load, and the change in the thermophysical properties are discussed in Sec. 3.1. The operating conditions of all the thermosyphons such as evaporator heat load, cooling water inlet temperature, and mass flow rate are maintained constant for effective comparison of results. The experimental conditions chosen for the present study is given in Table 1. The vapor and wall temperatures measured at the evaporator and condenser sections are given in Tables 2 and 3. The readings are taken for analysis and data reduction when steady-state temperature is reached.

The wall temperature distribution along the axial length of the thermosyphon for an average heat load of 30 W is shown in Fig. 4. It is clearly seen that a reduction in wall temperature is observed when the concentration of nanofluid increases. A reduction of about 21.4 °C is observed in the evaporator section of the thermosyphon for the maximum concentration of 0.09 vol. % when compared with that of acetone. Similarly, a drop of 8.8 °C is observed in the condenser wall temperature for the same concentration. This drop in wall temperature increases the operating range of thermosyphon when nanofluid is used. Figure 5 shows the variation in the adiabatic wall temperature with respect to the heat load. From Fig. 5, it is observed that the adiabatic wall temperature of the thermosyphon increases as heat load on the evaporator section increases, and it decreases as the volume concentration of nanoparticles in base fluid increases. A temperature

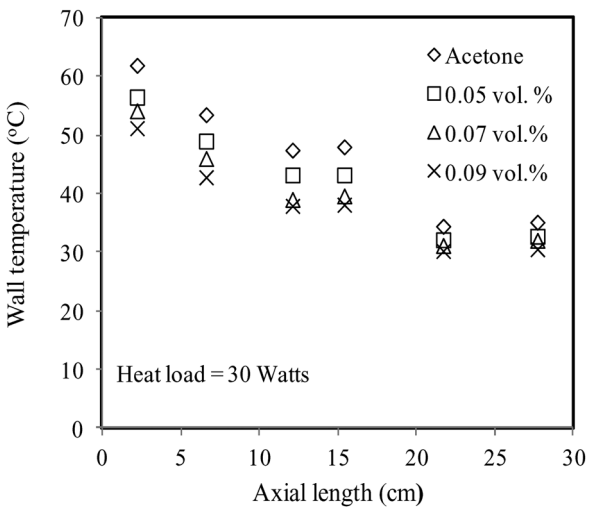

Fig. 4 Variation of wall temperature with respect to axial length

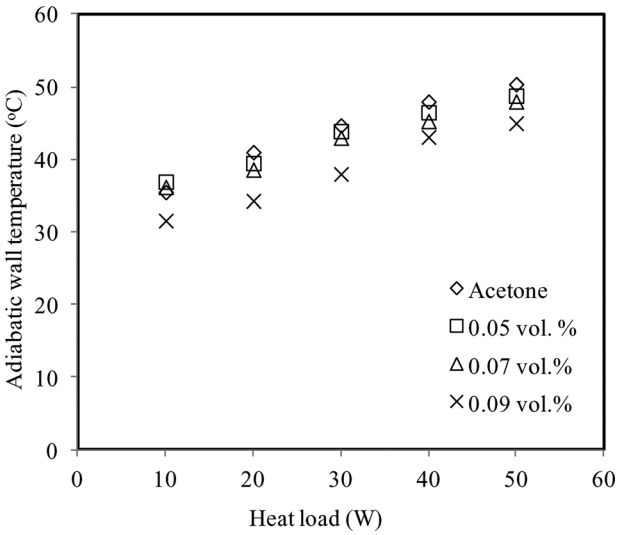

Fig. 5 Adiabatic wall temperature as a function of heat load

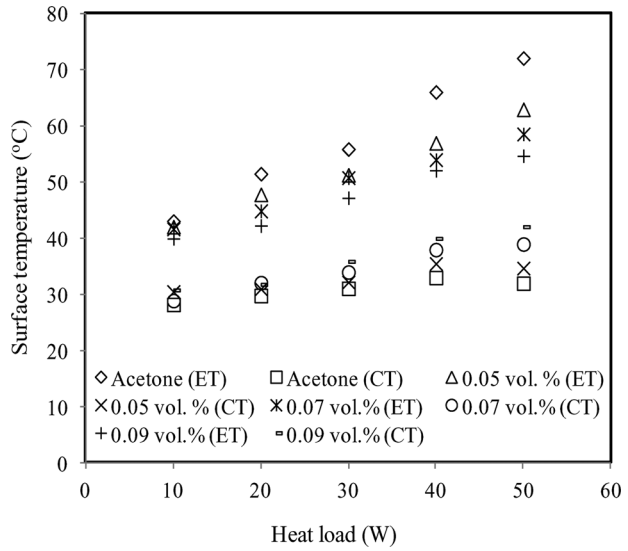

Fig. 6 Evaporator and condenser surface temperature as a function of heat load

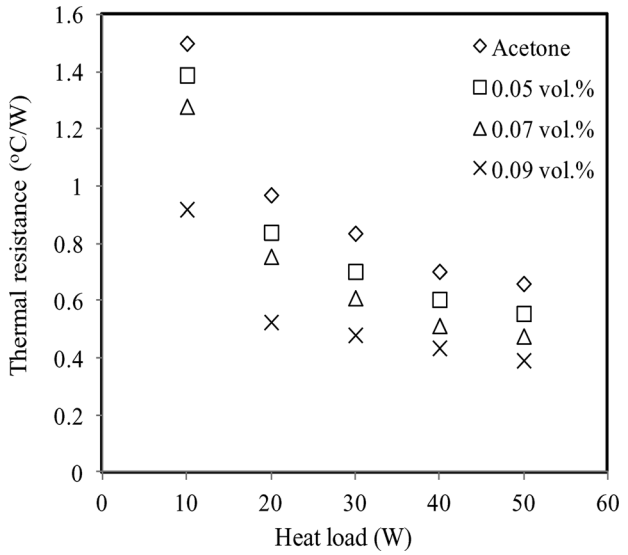

Fig. 8 Variation in thermal resistance as a function of heat load

reduction of 14.5% is observed in case of thermosyphon with 0.09% volume concentration and this is due to increase in the effective heat transfer capability of the nanofluid. Similarly, a reduction of 3.8% and 1.6% is observed, respectively, for 0.05% and 0.07% volume concentrations of graphene–acetone nanofluids when compared with that of the acetone.

Figure 6 shows the variation in the surface temperatures of evaporator and condenser with respect to the heat load. From Fig. 6, it is clearly observed that the evaporator wall temperature increases with increment in the heat load and decreases as the volume concentration of nanoparticles increases in the base fluid. This reduction in wall temperature enhances the dissipation of heat from the electronic devices. It is also found that a reduction in the evaporator wall temperature of about 17.4 °C is noted at the heat input of 50 W for 0.09% volume concentration. Similarly, a reduction in the temperature difference of 13.5 °C and 9.1 °C in evaporator wall temperatures is obtained for the volume concentrations of 0.07% and 0.05%, respectively, when compared with that of thermosyphon with acetone. It is also found that the condenser wall temperature increases due to the effective heat rejection in condenser section, when the volume concentration of nanoparticles in base fluid increases. Similarly, Kim et al. [20] indicated that during nucleate boiling some nanoparticles gets deposited on the evaporator heating surface and forms a porous layer which reduces the vapor temperature and increases the heating surface area. This results in reduction of temperature of the evaporator. Figure 7 shows the temperature difference between evaporator and condenser as a function of heat load. From the figure, it is observed that the temperature difference between evaporator and condenser gradually decreases with respect to the increase in the volume concentration of nanoparticles for a given heat load. The use of nanofluid allows the thermosyphon to operate at higher heat load, for a constant temperature difference between evaporator and condenser. It is also observed that the temperature difference reduces by 64.23%, 31.8%, and 19%, respectively, for 0.09%, 0.07%, and 0.05% volume concentrations of graphene–acetone nanofluid when compared to thermosyphon operating with acetone. This reduction in temperature difference enhances the heat transport capability of the thermosyphon. The

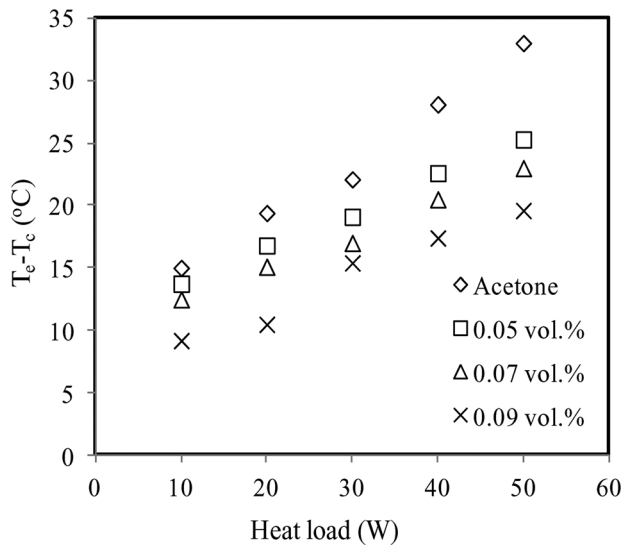

Fig. 7 Evaporator and condenser surface temperature difference as a function of heat load

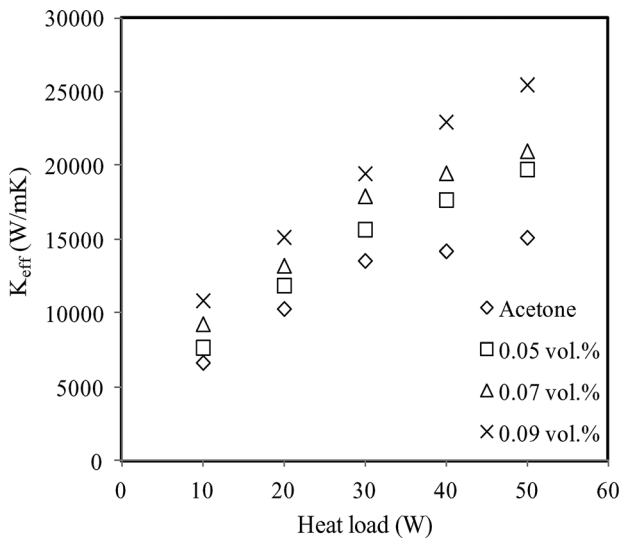

Fig. 9 Effective thermal conductivity of thermosyphon as a function of heat load

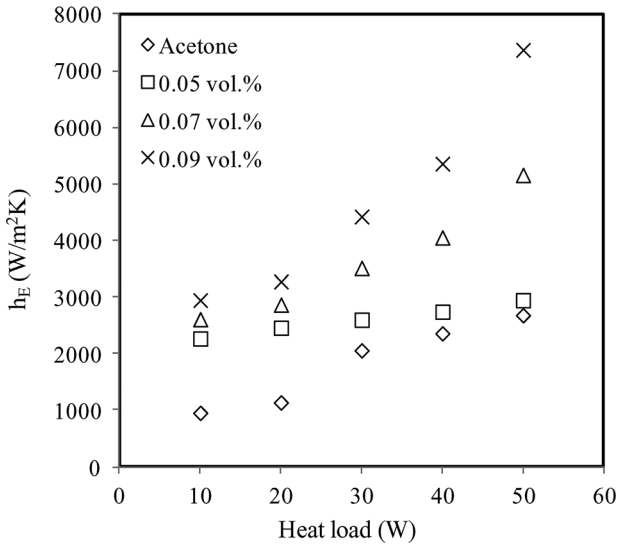

Fig. 10 Evaporator heat transfer coefficient with respect to heat load

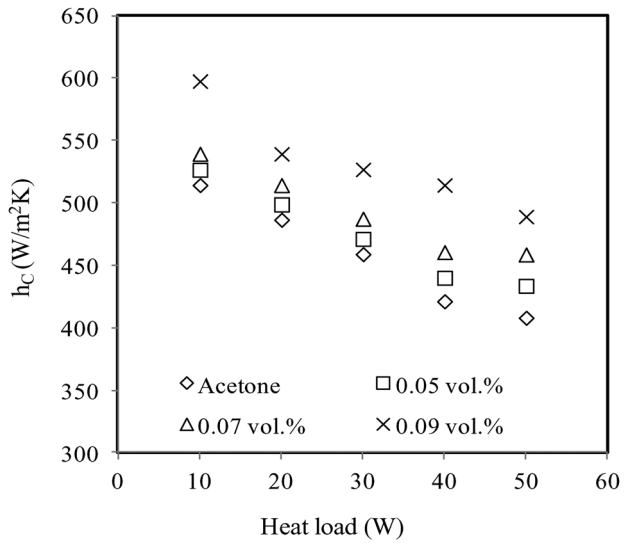

Fig. 11 Condenser heat transfer coefficient with respect to heat load

reason for this enhancement is attributed to be the formation of more nucleation boiling sites in the evaporator section due to addition of nanoparticles, which stimulate the boiling phenomena resulting in the enhanced heat transfer in the evaporator.

Figure 8 shows the variation in the thermal resistances of thermosyphon with different heat load for base fluid and nanofluid at different volumetric concentrations. The thermal resistances are calculated based on the wall temperatures to quantitatively evaluate the thermal performance of thermosyphon using graphene–acetone nanofluids. The thermal resistances are found to be high at lower heat loads; since a thick liquid film resides in the evaporator section and the same decreases as the heat load increases for both acetone and for nanofluids. A reduction in the thermal resistance of 70.3% is observed at 0.09 vol. % concentration when compared with that of the acetone, and the thermal resistance increases as the volume concentration of nanoparticle is reduced. It is also seen that 31.6% and 15.5% reduction in thermal resistance is observed for 0.07% and 0.05% volume concentrations of graphene–acetone nanofluid. However, for the maximum volume concentration of 0.09% of graphene–acetone nanofluid, 70.3% reduction in thermal resistance is observed when compared with acetone. The thermal resistance of thermosyphon is due to the formation of vapor bubble at the liquid–solid interface which results in larger bubble nucleation size, which prevents the transfer of heat from the solid surface to the liquid and creates high thermal resistance [21]. The suspended nanoparticles bombard with the vapor bubble during the bubble formation. Therefore, it is expected that the nucleation size of the vapor bubble is smaller for nanofluids than base fluids.

Figure 9 shows the effective thermal conductivity of thermosyphon with respect to various heat loads. It is observed that the effective thermal conductivity increases with the increase in the heat load and volume concentration. An enhancement of 56.72% is observed for 0.09 vol. % concentration of graphene–acetone nanofluid. This concludes that the effective heat transfer is possible through the thermosyphon employed with nanofluids. Similarly, the thermosyphon with 0.07 vol. %and 0.05 vol. % gives 35.13% and 20.26% increment in the effective thermal conductivity when compared with acetone based thermosyphon. Figure 10 shows the evaporation heat transfer coefficient as a function of heat load. It is observed that the evaporation heat transfer coefficient of thermosyphon with graphene–acetone nanofluid is higher when compared with that of the thermosyphon with pure acetone for the same heat load. The heat transfer coefficient increases with increasing volume concentration of the nanoparticle in base fluid. An increment of 61.25% in evaporation heat transfer coefficient is observed at 0.09% volume concentration when compared to base fluid. It is due to the less temperature difference between the evaporator wall and vapor core with the use of nanofluids. The nanofluids can enhance the heat transfer with different reasons: the addition of nanoparticles to base fluid changes the heat transfer mechanism so that the thermal conductivity increases the Brownian motion, dispersion, and fluctuation of the nanoparticles near the wall which leads to an increase in the energy exchange rates [22]. Besides, due to the temperature gradient available in the mixture, the particles tend to move in the direction of decreasing temperature (thermophoresis). Also, the concentration gradient available in the solution causes the particles to immigrate to a zone with lower concentration (diffusiophoresis or osmophoresis). These interactions cause the heat transfer rate to increase. In the present study, the evaporator section is heated until the wall temperature is increased above the saturation temperature of the nanofluid. This causes the separation of the isolated bubbles formed at the nucleation sites and hence induces considerable fluid mixing and fluctuation of nanoparticles near the wall, which therefore leads to an increase in the energy exchange rates and augments the heat transfer rate between the fluid and the evaporator section wall. This concludes that the effective heat transfer is possible through thermosyphon employed with nanofluids as working fluid.

Figure 11 shows the heat transfer coefficient of a condenser with respect to heat load. It is observed that the heat transfer coefficient in the condenser section decreases for both acetone and for nanofluid with increasing heat load. It is also observed that the use of nanofluid increases the heat transfer coefficient of condenser when compared with that of acetone. An increment in the condenser heat transfer coefficient of 85.74% is obtained for 0.09% volume concentration of nanoparticles compared with that of the acetone. From the above results, it is clearly observed that the presence of nanoparticles decreases the wall and the vapor temperatures which, in turn, increase the operating range of the thermosyphon to higher heat load. Dispersion of a small volume concentration of nanoparticles in the base fluid enhances the thermal performance of the thermosyphon when compared with that of the pure fluid.

3.2 Visualization of Flow Pattern. The visualization study of the flow pattern in the vertical thermosyphon is carried out by keeping the mass flow rate, inlet water temperature of condenser

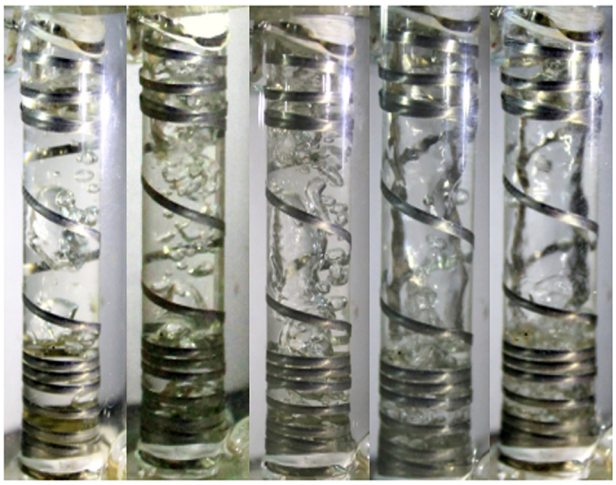

Fig. 12 Flow regimes at evaporator section of thermosyphon at different heat load

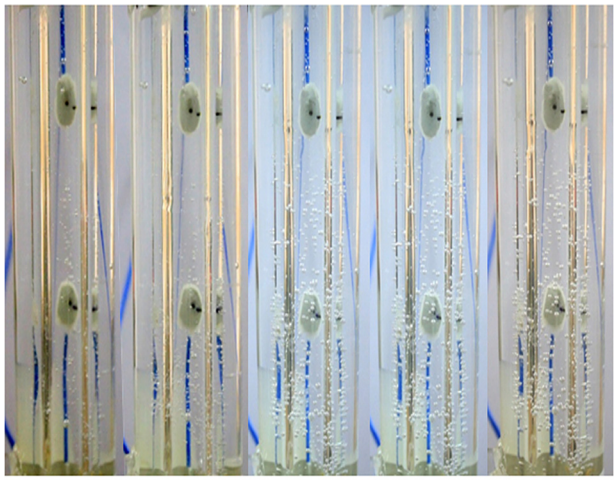

Fig. 14 Condensation section of thermosyphon at different heat load

as constant. Figure 12 shows the flow regimes in the evaporator section of thermosyphon at different heat loads. It is observed that due to the variation in the heat load from 10 W to 50 W, the natural convection in the evaporator region results in the phase change of the working fluid. At the initial condition, before applying the heat load at the evaporator the acetone is in pure liquid state. As the heat load increases in the evaporator, say at 10 W the wall temperature increases above the saturation temperature of the working fluid at the given pressure. At this stage, discrete bubbles are formed in a continuous liquid phase. These bubbles having the mean size less than the diameter of the tube is observed and the number of bubbles formed is less. At 20 W small bubbles are formed and the number of bubbles increases. The bubbles create a lot of agitation and mixing near the wall, which enhances heat transfer rate of the thermosyphon as the heat load increases. Further, increase in the heat load of 30 W, the quality increases to intermediate stage and the smaller bubbles coalesces and the vapor shear on to the liquid–vapor interface tends to be unstable and oscillatory which is referred as churn flow. The flow regime observed at 40 W and 50 W is annular flow. In this flow regime the liquid is expelled from the centre of the tube and flows as thin film on the wall, forming an annular ring of liquid. In addition, it is well known that in the two-phase flow study, the annular flow pattern results in a higher heat transfer coefficient when compared to other flow patterns. Similarly in the present study, at higher heat loads of (40 W and 50 W), the annular flow pattern is observed resulting in a higher heat transfer coefficient in the evaporator section.

Figure 13 shows the flow pattern of adiabatic section of the thermosyphon at different heat loads. From all the images, it is clearly observed that the flow pattern is the slug flow. The bubbles from the evaporator section collide and coalesce to form large bubble, which are similar in dimension to the tube. These bubbles have a shape similar to a bullet with a hemispherical nose with a blunt tail end. It is also observed that the liquid film thickness at the wall of the adiabatic section increases as the heat load at the evaporator of thermosyphon increases. This is due to the fall of liquid due to gravity from the condenser section after cooling.

Figure 14 shows the flow pattern in the condenser section of the thermosyphon at different heat loads. The outer shell of the condenser section is filled with cold water. In the condenser section, the condensation of vapor takes place between the vapor in the condenser section and the cooling water circulated in the shell side of the condenser section. Since the condenser section is surrounded by a water cooled heat exchanger, the vapor could not be visualized. However, the thermocouples are fixed to measure the vapor temperature in the condenser section. From the thermocouple reading, it is clearly observed that an increase in the outlet temperature of the cooling water is observed from the shell side of the condenser section. The condensed acetone from the condenser section falls back to the evaporator section through the walls of the thermosyphon due to gravity. It is clear from the figure that the bubbles are formed on the walls of the condenser section, where the cold water is circulated. The bubble formation is due to the heat transfer from the wall to the cold water. It is clearly observed that the number of bubbles inside the shell side of the condenser increases as the heat load increases.

Fig. 13 Flow regimes at adiabatic section of thermosyphon at different heat load

4 Conclusion

The present experimental work reported that the use of low volume concentration of graphene nanoparticles in acetone enhances the heat transfer performance of the thermosyphon effectively. The thermal resistance of thermosyphon is decreased by 70.3% with the use of graphene–acetone nanofluid, which in turn

increased the effective thermal conductivity by 37.3%. A temperature difference of 4.62 °C, 3.28 °C, 2.78 °C, and 1.8 °C is, respectively, observed between the wall and vapor core at the evaporation section for acetone, 0.05 vol. %, 0.07 vol. %, and 0.09 vol. % concentrations of graphene nanoparticles, indicating the improved performance of the thermosyphon. The evaporation and condensation heat transfer coefficient also increased with increasing graphene nanoparticles concentrations. The higher thermal performance of thermosyphon working with nanofluid proved its potential as a substitute for conventional fluids and makes nanofluid attractive as an advanced heat transfer fluid for electronic cooling applications.

Acknowledgment

The authors would like to thank Mr. R. Jeya seelan, of Karunya University for helping in the fabrication of the experimental test facility. The second author wishes to express his indebtedness to the National Science and Technology Development Agency, the Thailand Research Fund, and the National Research University Project for supporting his study.

Nomenclature

A = surface area (m^2)
C_p = specific heat (J/kg K)
d = outer diameter (m)
E_{SURF} = evaporator surface temperature (°C)
E_{VAP} = evaporator surface temperature (°C)
h = heat transfer coefficient (W/m^2 K)
K = thermal conductivity (W/m K)
L = length (m)
M = mass flow rate (kg/s)
Q = heat load (W)
Q = heat flux (kW/m^2)
R = thermal resistance (°C/W)
T = average temperature (°C)
$U(\Delta T)$ = uncertainty value in the temperature difference between the evaporator and condenser (°C)
ΔT = temperature difference (°C)

Subscripts

a = adiabatic
c = condenser
c/s = cross-sectional
ct = condenser temperature
cw = cooling water
e = evaporator
ec = evaporator and condenser
eff = effective
et = evaporator temperature
T = thermosyphon
Inlet = inlet to condenser
nf = nanofluid
p = particle
Surf = surface
v = vapor
Vs = vapor and surface
w = wall
W = water

Greek Symbols

φ = volume fraction
ρ = density (kg/m^3)

References

[1] Ivanova, M., Avenas, Y., Schaeffer, C., Dezord, J. B., and Harder, J. S., 2006, "Heat Pipe Integrated in Direct Bonded Copper (DBC) Technology for Cooling of Power Electronics Packaging," IEEE Trans. Power Electron., **21**(6), pp. 1541–1547.
[2] Leong, K. Y., Saidur, R., Mahlia, T. M. I., and Yau, Y. H., 2012, "Performance Investigation of Nanofluids as Working Fluid in a Thermosyphon Air Preheater," Int. Commun. Heat Mass Transfer, **39**(4), pp. 523–529.
[3] Shafai, M., Bianco, V., Vafai, K., and Manca, O., 2010, "An Investigation of Thermal Performance of Cylindrical Heat Pipe Using Nanofluids," Int. J. Heat Mass Transfer, **53**(1–3), pp. 376–383.
[4] Buschmann, M. H., and Franzke, U., 2014, "Improvement of Thermosyphon Performance by Employing Nanofluid," Int. J. Refrig., **40**, pp. 416–428.
[5] Pang, C., Jung, J. Y., Lee, J. W., and Kang, Y. T., 2012, "Thermal Conductivity Measurement of Methanol-Based Nanofluids With Al2O3 and SiO2 Nanoparticles," Int. J. Heat Mass Transfer, **55**(21–22), pp. 5597–5602.
[6] Longo, G. A., and Zilio, C., 2011, "Experimental Measurement of Thermophysical Properties of Oxide–Water Nano-Fluids Down to Ice-Point," Exp. Therm. Fluid Sci., **35**(7), pp. 1313–1324.
[7] Baby, T. T., and Ramaprabhu, S., 2010, "Investigation of Thermal and Electrical Conductivity of Graphene Based Nanofluids," J. Appl. Phys., **108**(12), p. 124308.
[8] Murshed, S. M. S., Leong, K. C., and Yang, C., 2008, "Investigations of Thermal Conductivity and Viscosity of Nanofluids," Int. J. Therm. Sci., **47**(5), pp. 560–568.
[9] Shabgard, H., Xiao, B., Faghri, A., Gupta, R., and Weissman, W., 2014, "Thermal Characteristics of a Closed Thermosyphon Under Various Filling Conditions," Int. J. Heat Mass Transfer, **70**, pp. 91–102.
[10] Noie, S. H., Heris, S. Z., Kahani, M., and Nowee, S. M., 2009, "Heat Transfer Enhancement Using Al_2O_3/Water Nanofluid in a Two-Phase Closed Thermosyphon," Int. J. Heat Fluid Flow, **30**(4), pp. 700–705.
[11] Huminic, G., Huminic, A., Morjan, I., and Dumitrache, F., 2011, "Experimental Study of the Thermal Performance of Thermosyphon Heat Pipe Using Iron Oxide Nanoparticles," Int. J. Heat Mass Transfer, **54**(1–3), pp. 656–661
[12] Kang, S. W., Wei, W. C., Tsai, S. H., and Yang, S. Y., 2006, "Experimental Investigation of Silver Nano-Fluid on Heat Pipe Thermal Performance," Appl. Therm. Eng., **26**(17–18), pp. 2377–2382
[13] Asirvatham, L. G., Nimmagadda, R., and Wongwises, S., 2013, "Heat Transfer Performance of Screen Mesh Wick Heat Pipes Using Silver–Water Nanofluid," Int. J. Heat Mass Transfer, **60**, pp. 201–209
[14] Karthikeyan, M., Vaidyanathan, S., and Sivaraman, B., 2010, "Thermal Performance of a Two Phase Closed Thermosyphon Using Aqueous Solution," Int. J. Eng. Sci. Technol., **2**(5), pp. 913–918.
[15] Mozumder, A. K., Akon, A. F., Chowdhury, M. S. H., and Banik, S. C., 2010, "Performance of Heat Pipe for Different Working Fluids and Filling Ratios," J. Mech. Eng., **41**(2), pp. 96–102.
[16] Naphon, T., and Assadamongkol, P., 2008, "Heat Pipe Efficiency Enhancement With Refrigerant-Nanoparticles Mixtures," J. Energy Convers. Manage., **50**(3), pp. 772–776.
[17] Khandekar, S., Charoensawan, P., Groll, M., and Terdtoon, P., 2003, "Closed Loop Pulsating Heat Pipes Part B: Visualization and Semi-Empirical Modeling," Appl. Therm. Eng., **23**(16), pp. 2021–2033.
[18] Pak, B. C., and Cho, I. Y., 1998, "Hydrodynamic and Heat Transfer Study of Dispersed Fluids With Sub-Micron Metallic Oxide Particles," Exp. Heat Transfer, **11**(2), pp. 151–170.
[19] Godson, L., Raja, B., lal, D. M., and Wongwises, S., 2010, "Experimental Investigation on the Thermal Conductivity and Viscosity of Silver-Deionized Water Nanofluid," Exp. Heat Transfer, **23**(4), pp. 317–332.
[20] Kim, H. D., Kim, J., and Kim, M. H., 2007, "Experimental Studies on CHF Characteristics of Nano-Fluids at Pool Boiling," Int. J. Multiphase Flow, **33**(7), pp. 691–706.
[21] Collier, J. G., and Thome, J. R., 1996, *Convective Boiling and Condensation*, Clarendon Press, Oxford, UK.
[22] Zeinali Heris, S., Nasr Esfahany, M., and Etemad, G., 2006, "Investigation of CuO/Water Nanofluid Laminar Convective Heat Transfer Through a Circular Tube," J. Enhanced Heat Transfer, **13**(4), pp. 279–289.